

Supporting Information

Major et al. 10.1073/pnas.0911416106

SI Text

Additional details of X-ray crystal structure determination and computational results for the reaction catalyzed by nitroalkane oxidase (Fig. S1) are described in this text. The input, topology, parameter, and coordinate files for the simulation of the nitroalkane oxidase reaction presented in this article will be provided upon request because these files are too large to be included here. These files can be directly used with CHARMM, version c34a1.

Data collection and refinement statistics are given in Table S1. The complete data has been collected to 2.40-Å resolution.

Configurations Used in Michaelis Complex Optimization. Fig. S2A illustrates the initial 10 configurations of the substrate, superimposed in the active site of nitroalkane oxidase (PDB ID code 1C12), which were used to model the Michaelis complex structure in molecular dynamics simulations. Fig. S2B depicts the final configurations, superimposed in the same orientation as in Fig. S2A, after 100-ps molecular dynamics simulations for each configuration.

Effective potentials for tunneling, which is the vibrationally adiabatic ground-state potential energy including the changes in zero-point energies of modes transverse to the reaction coordinate, are functions of distance s along the minimum energy path (1–7). Harmonic frequencies were determined by first projecting out the degrees of freedom corresponding to the reaction coordinate s before diagonalization of the Hessian (8). The effective potentials are normalized to zero at their saddle points.

All calculations were performed using CHARMMRATE that integrates CHARMM and POLYRATE (9).

Crystal Structure Determination. The wild-type and the D402N mutant enzymes were expressed in *E. coli* and purified as described in ref. 10. Protein concentrations were determined using the ϵ_{446} value of $14.2 \text{ mM}^{-1} \text{ cm}^{-1}$. Crystals of D402N with nitroethane were obtained using hanging drop vapor-diffusion methods similar to those described in refs. 11–13 with the exception that spermine was omitted. Typically, $1 \mu\text{l}$ of 1-nitroethane was added to $50 \mu\text{l}$ of stock enzyme solution ($\approx 10 \text{ mg/ml}$) immediately before setting up the drops. The crystals were grown at 277 K from a mother liquor solution containing 24–30% (wt/vol) PEG4000 or PEG3350, 20% (vol/vol) glycerol, 100 mM sodium cacodylate, pH 7.5. The crystals were harvested with nylon loops and were flash frozen by quick submersion in liquid nitrogen without further cryoprotection. X-ray diffraction data collection was at beamline X29 of the National Synchrotron Light Source with crystals held at 100 K. Data were integrated and scaled with HKL2000 (14). The structures were solved by molecular replacement with PHASER from the CCP4 suite of programs. Initially the search models comprised a monomer extracted from the wild-type NAO structure (PDB ID code 2c0u) (11) from which all solvent and FAD atoms were removed. The solutions indicated that the crystals were in space group $P3_221$ with one $\alpha 4$ holoenzyme in the asymmetric unit. Model refinement was with REFMAC 5.2 without using noncrystallographic symmetry restraints. Data collection and model refinement statistics are presented in Table S1.

1. Isaacson AD, Truhlar DG (1982) Polyatomic canonical variational theory for chemical reaction rates. Separable-mode formalism with application to $\text{OH} + \text{H}_2 \rightarrow \text{H}_2\text{O} + \text{H}$. *J Chem Phys* 76:1380–1391.
2. Garrett BC, Truhlar DG (1979) Generalized transition state theory. Canonical variational calculations using the bond energy-bond order method for bimolecular reactions of combustion products. *J Am Chem Soc* 101:5207–5217.
3. Garrett BC, Truhlar DG (1980) Improved canonical variational theory for chemical reaction rates. Classical mechanical theory and applications to collinear reactions. *J Phys Chem* 84:805–812.
4. Truhlar DG, Garrett BC (1980) Variational transition-state theory. *Accounts Chem Res* 13:440–448.
5. Truhlar DG, et al. (1992) Variational transition-state theory and multidimensional, semiclassical, ground-state transmission coefficients. Applications to secondary deuterium kinetic isotope effects in reactions involving methane and chloromethane. *Am Chem Soc Symp Ser* 502:16–36.
6. Liu YP, et al. (1993) Direct dynamics calculation of the kinetic isotope effect for an organic hydrogen-transfer reaction, including corner-cutting tunneling in 21 dimensions. *J Am Chem Soc* 115:7806–7817.
7. Fernández-Ramos A, Truhlar DG (2001) Improved algorithm for corner-cutting tunneling calculations. *J Chem Phys* 114:1491–1496.
8. Alhambra C, et al. (2001) Canonical variational theory for enzyme kinetics with the protein mean force and multidimensional quantum mechanical tunneling dynamics. Theory and application to liver alcohol dehydrogenase. *J Phys Chem B* 105:11326–11340.
9. Garcia-Viloca M, et al. (2002) CHARMMRATE (a module of CHARMM) (University of Minnesota, Minneapolis), Version 2.
10. Valley MP, Fitzpatrick PF (2003) Reductive half-reaction of nitroalkane oxidase: Effect of mutation of the active site aspartate to glutamate. *Biochemistry* 42:5850–5856.
11. Nagpal A, Valley MP, Fitzpatrick PF, Orville AM (2006) Crystal structures of nitroalkane oxidase: Insights into the reaction mechanism from a covalent complex of the flavoenzyme trapped during turnover. *Biochemistry* 45:1138–1150.
12. Fitzpatrick PF, et al. (2007) Mechanistic and structural analyses of the roles of Arg409 and Asp402 in the reaction of the flavoprotein nitroalkane oxidase. *Biochemistry* 46:13800–13808.
13. Nagpal A, Valley MP, Fitzpatrick PF, Orville AM (2004) Crystallization and preliminary analysis of active nitroalkane oxidase in three crystal forms. *Acta Crystallogr D* 60:1456–1460.
14. Otwinowski Z, Minor W (1997) Processing of x-ray diffraction data collected in oscillation mode. *Methods Enzymol* 276:307–326.

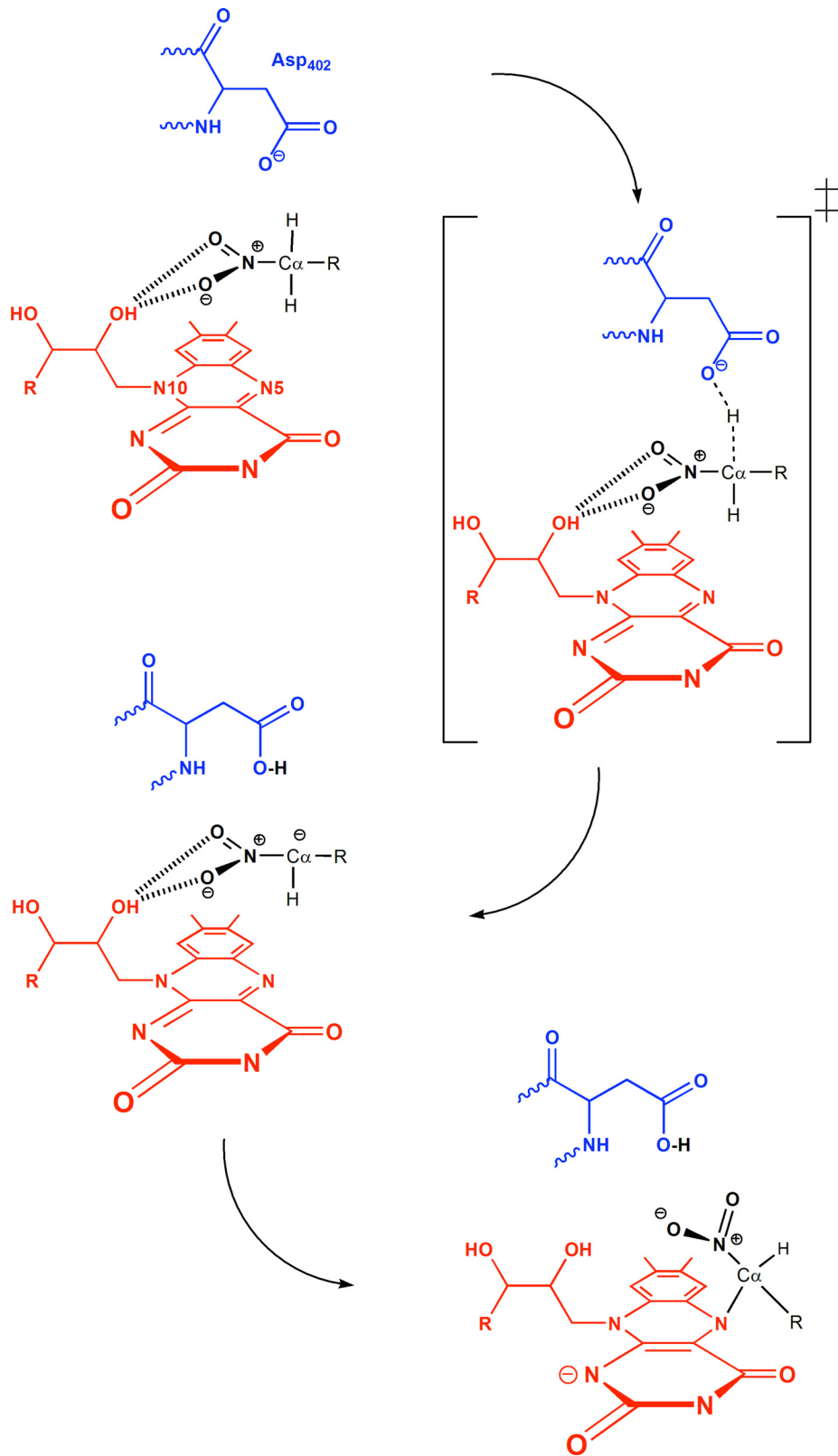


Fig. S1. Reaction pathway catalyzed by nitroalkane oxidase.

Table S1. Crystal structure data collection and refinement statistics

NAO isoform	D402N
Ligand(s)	NO ₂ -ethane
Wavelength, Å	1.0809
Space group	<i>P</i> 3 ₂ 21
<i>a</i> (Å), <i>b</i> (Å), <i>c</i> (Å)	108.8, 108.8, 340.9
Resolution range, Å	30–2.40
Highest-resolution shell, Å	2.80–2.10
Total observations	325,283
Unique observations	91,770
Completeness, %	98.9 (99.9)*
Redundancy	3.5 (3.7)*
<i>R</i> _{sym} , % [†]	10.0 (54.3)*
<i>I</i> / σ <i>I</i>	22.2 (2.7)*
Model refinement statistics	
Total number of nonhydrogen atoms	13,859
No. protein/ligand/water nonhydrogen atoms	1,724/16/650
Resolution range, Å	30–2.4
<i>R</i> _{cryst} , % [‡]	19.7 (25.1)*
<i>R</i> _{free} , % [§]	25.1 (33.9)*
Estimated overall coordinate error based on <i>R</i> value, Å	0.32
Correlation coefficient (<i>F</i> _o – <i>F</i> _c)	0.952
rmsd from ideal geometry	
Bond lengths, Å	0.014
Bond angles, °	1.51

*Highest-resolution shell.

[†] $\sum (|I_{hkl} - \langle I_{hkl} \rangle|) / \sum I_{hkl}$.

[‡]*R* value calculated with the working and the test set inclusive.

[§]Free *R* value test set calculated with 5% of the data.